

Incremental Multi-Scene Modeling via Continual Neural Graphics Primitives

Prajwal Singh

Ashish Tiwari

Gautam Vashishtha

Shanmuganathan Raman

CVIG Lab, IIT Gandhinagar, India

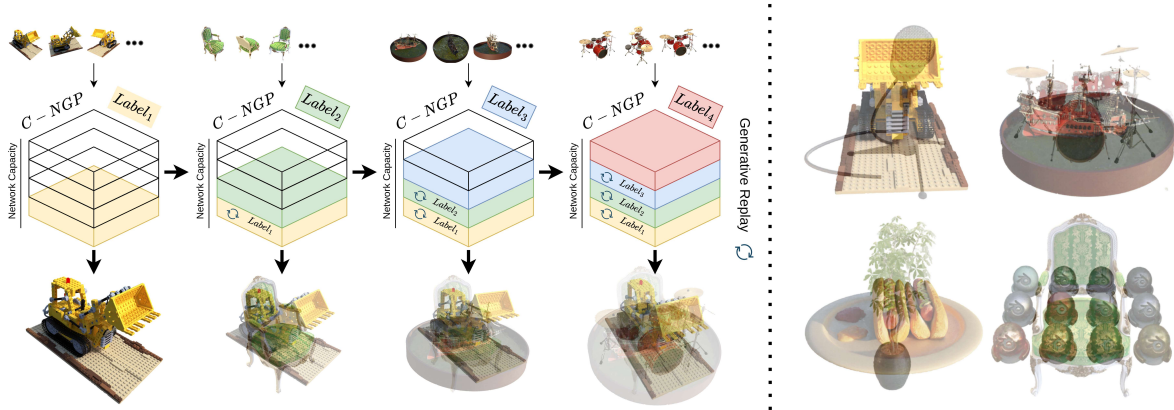
`{singh_prajwal, ashish.tiwari, gautam.pv, shanmuga}@iitgn.ac.in`

Figure 1. (Left) The proposed continual neural graphics primitives (C-NGP) framework to model multiple scenes. Every new scene is assigned a unique pseudo-label and trained sequentially while preserving the previously learned information via generative replay. Any specific scene can be rendered by conditioning C-NGP over the associated pseudo-label. (Right) We visualize the learned multi-scene radiance field where 8 scenes from the NeRF Synthetic 360° [37] dataset are shown as separate pairs for clarity.

Abstract

Neural radiance fields (NeRF) have revolutionized photorealistic rendering of novel views for 3D scenes. Despite their growing popularity and efficiency as 3D resources, NeRFs face scalability challenges due to the need for separate models per scene and the cumulative increase in training time for multiple scenes. The potential for incrementally encoding multiple 3D scenes into a single NeRF model remains largely unexplored. To address this, we introduce Continual-Neural Graphics Primitives (C-NGP), a novel continual learning framework that integrates multiple scenes incrementally into a single neural radiance field. Using a generative replay approach, C-NGP adapts to new scenes without requiring access to old data. We demonstrate that C-NGP can accommodate multiple scenes without increasing the parameter count, producing high-quality novel-view renderings on synthetic and real datasets. Notably, C-NGP models all 8 scenes from the Real-LLFF dataset together, with only a 2.2% drop in PSNR compared to vanilla NeRF, which models each scene independently. Further, C-NGP allows multiple style edits in the same network. The implementation details and dynamic visualizations are in the supplementary material.

1. Introduction

Neural Radiance Fields (NeRF) synthesize novel photorealistic views from a set of input images by modeling 3D scenes via Multi-Layer Perceptrons (MLPs) and differentiable volumetric rendering. Despite their strengths, NeRF and its variants suffer from extensive per-scene optimization and long training times. Recent advancements have addressed these limitations by accelerating training through caching or sparse voxel grids [17, 58, 67], reducing inference time [12, 56], compressing models [9, 16, 19, 48, 52], enabling scene editing [2, 60], improving generalization [10, 22, 59, 65, 67, 71], and supporting few-shot learning [28, 57, 66]. However, encoding multiple scenes within a single NeRF model remains largely under-explored. Having to train separate NeRFs for each scene significantly increases storage and training time. Developing a single radiance field to accommodate multiple scenes with the same number of parameters would enhance the scalability and applicability of NeRFs as 3D assets. Modeling multiple scenes efficiently requires: (a) photorealistic rendering of all observed scenes, (b) adding new scenes without requiring previous training data, (c) preserving learned knowledge, and (d) maintaining a fixed parameter count.

To address this, we draw inspiration from continual learning to accommodate new scenes while minimizing interference with previously learned ones. Specifically, we use conditioning to define a separate parameter subspace for each scene, ensuring that new scenes are integrated smoothly without overlapping with existing representations. However, integrating continual learning with NeRF to represent multiple scenes is difficult due to the underlying fundamental differences. For example, unlike image classification, where an image seldom has different labels, the same position and view direction across different scenes modeled by NeRF will have different densities and colors. Additionally, classification models learn reusable features across tasks, while NeRF requires scene-specific representations.

To leverage feature reuse, some methods [3, 8, 22, 59, 65] integrate convolutional feature extractors to learn local and global scene features [4, 41, 67], along with attention modules, 3D cost volume features, and other advanced neural networks. These approaches focus on faster optimization and improved generalizability but are not designed for incremental scene integration and suffer from catastrophic forgetting of previously trained scenes. While some studies have explored combining continual learning with NeRF [7, 13, 42, 68], they are limited to single-scene reconstruction with variations in appearance or geometry over time. In contrast, we aim to enable NeRF models to represent multiple distinct scenes using a shared parameter with continual learning.

In this work, we propose **Continual Neural Graphics Primitives (C-NGP)** to model multiple scenes within a single radiance field. C-NGP leverages the fast training and efficient learning of Instant-NGP [38] by integrating scene conditioning into its hashing mechanism using pseudo-labels to maximize the use of a single NGP parameter space for multiple scenes. This simple yet effective conditioning enables multi-scene optimization, allowing the model to learn new scenes while preserving high-fidelity rendering of previously encountered ones without relying on any pre-trained priors or feature extraction blocks. By leveraging the generative-replay paradigm, C-NGP can accommodate new scenes without requiring access to training data from previously learned scenes. Therefore, C-NGP becomes more practical for real-world applications, especially in scenarios with limited training data and resources, as it models multiple 3D scenes without additional computational overhead or extensive re-training.

The key contributions of our work are listed below.

- We present C-NGP, the first approach to continually encode multiple scenes in a single radiance field with a fixed parameter count and reasonably low, if not no, loss in rendering quality of the previously learned scenes. We observe merely a 2.2% drop in PSNR over all the scenes from the Real-LLFF dataset [36] compared to the scene-specific

vanilla NeRF.

- Using generative replay, we eliminate C-NGP’s dependence on past training data.
- C-NGP adapts to diverse scenes through a simple yet effective scene conditioning mechanism integrated into the hashing structure of Instant-NGP [38]
- Further, we demonstrate that the C-NGP framework allows for multi-view consistent style editing incorporating multiple-edit styles in the same network.
- C-NGP consistently outperforms existing related methods over multi-scene rendering quality, training efficiency, and adaptability to new scenes.

Interestingly, we observed that even the vanilla NeRF, under the proposed continual learning paradigm, can model multiple scenes, except that it takes a massive amount of training time and offers lower performance than C-NGP.

2. Related Work

Novel View Synthesis. Generating novel views from limited 2D observations is a key problem in computer vision and graphics [54]. Traditional methods without explicit 3D structure representation require densely sampled viewpoints for photorealistic rendering [14, 20, 29]. Some approaches use voxel-based representations to encode 3D spatial structures, but they suffer from limited resolution and high memory demands [6, 31, 49, 63]. To reduce memory overhead, compact implicit representations like signed distance functions (SDFs) map spatial coordinates to 3D surfaces [35, 40, 41]. Neural Radiance Fields (NeRF) [37] have gained popularity for encoding scene geometry and synthesizing novel views. NeRF uses MLPs to estimate color and density at 3D points, enabling photorealistic rendering via volumetric integration. However, NeRF requires long per-scene optimization times. Faster alternatives, such as Plenoxels [17] and Instant-NGP [38], improve training efficiency using spherical harmonics, multi-resolution hash encoding, and fused MLPs. Other NeRF extensions aim at faster inference [12, 56], 3D scene editing [2, 60], and rendering from sparse images [28, 57, 66]. However, these methods focus on single-scene optimization without accommodating multiple scenes in a shared parameter space. Another line of work [10, 22, 59, 65, 67, 71] aims for generalization by pre-training NeRF models on multiple scenes. Still, they require fine-tuning on unseen scenes and suffer from forgetting previously learned ones, considering the shared parameter space. Many of these methods rely on CNN-based or 3D cost volume-based feature extractors, increasing computational and memory overhead due to additional learnable parameters.

In contrast, we propose a continual NGP paradigm where multiple scenes share the same parameter space. By applying pseudo-labels during training, our method enables scene-specific rendering without extra computational overhead

while preserving high fidelity for previously learned scenes.

NeRF and Continual Learning. Continual learning is a fundamental challenge in machine learning, requiring models to learn sequentially from new data without forgetting previously acquired knowledge [46]. In the context of NeRFs, traditional continual learning techniques focus on handling distribution shifts without retaining past data. Existing approaches fall into three broad categories: parameter isolation, regularization, and replay [7, 25, 30, 33, 45, 47]. However, these methods are not directly applicable to NeRF for multi-scene modeling due to the significant domain gap between different scenes, making parameter reuse inefficient. While some approaches work for within-scene transitions [7, 42, 68], they fail in multi-scene continual learning.

The SLAM-based methods such as [11, 15, 50] assume that past training data remains available to optimize over all keyframes in bundle adjustment. Other methods, such as MEIL-NeRF [13] and CLNeRF [7], reconstruct a scene incrementally from multiple partial scans but are limited to single-scene scenarios and only address forgetting within specific regions of a scene. In contrast, our approach enables continual learning across multiple distinct scenes.

A concurrent work, SCARF [61], also attempts to encode multiple scenes in NeRF using a hyper-network to generate scene-specific weights for the NeRF MLP. However, SCARF represents scenes as a combination of a cross-scene weight matrix and scene-specific weight matrices generated from a global parameter generator, requiring separate auxiliary networks. This results in increasing parameters with each new scene. In contrast, our approach maintains a fixed number of parameters and achieves fast convergence.

3. Method

We present C-NGP, a framework to incrementally model multiple scenes with the same set of parameters traditionally used for single-scene modeling in an NGP model. We begin with a brief overview of learning neural radiance fields and the multi-resolution hash encoding (MHE) technique. Next, we explore the conditional capabilities of Instant-NGP and describe how generative replay [47] can be integrated into conditional Instant-NGP. This extension enables incremental learning of new scenes while preserving information from previously encountered scenes. Finally, we discuss the associated training details.

3.1. Background

3.1.1. Neural Radiance Fields

Mildenhall *et al.* [37] introduced NeRF, a method for synthesizing novel views from a set of input images. It employs a multi-layer perceptron (MLP) that maps a 5D input, 3D spatial coordinates (x, y, z) and viewing direction (θ, ϕ) , to the density σ and color c of a point. These points are sampled

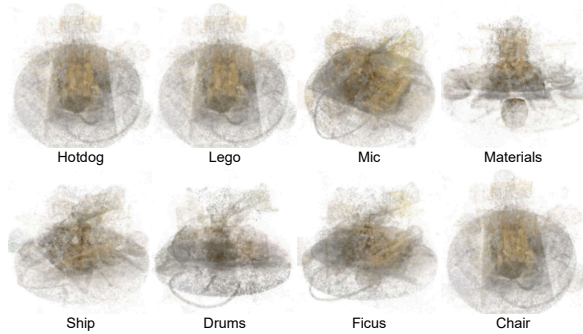


Figure 2. **Vanilla Instant-NGP** [38]. We combine different scenes of the NeRF Synthetic 360° [37] dataset and train Instant-NGP. The results show that neural hash encoding of scene coordinates may not be sufficient to preserve information across multiple scenes.

along camera rays, defined as $\mathbf{r}(t) = \mathbf{o} + t\mathbf{d}$, where \mathbf{o} is the camera origin, \mathbf{d} is the ray direction, and t is the sampled depth. Rendering is performed using volumetric integration [34]:

$$\hat{C}(r) = \sum_{i=1}^N w_i c_i, \tag{1}$$

where weights $w_i = T_i \alpha_i$ account for transmittance T_i and opacity $\alpha_i = (1 - e^{-\sigma_i \delta_i})$, with δ_i as the distance between adjacent samples. The model is optimized by minimizing the squared error between rendered and ground-truth pixel colors:

$$\mathcal{L} = \sum_{r \in \mathcal{R}} \|\hat{C}(r) - C(r)\|_2^2, \tag{2}$$

where \mathcal{R} is the set of rays. A sinusoidal positional encoding is applied to the inputs before passing them to the MLP.

3.1.2. Multi-Resolution Hash Encoding

Müller *et al.* [38] introduced the concept of multi-resolution hash encoding (MHE) to enhance both the reconstruction accuracy and training efficiency of neural radiance fields (NeRFs) while maintaining minimal computational overhead. Unlike the traditional positional encoding used in NeRF, MHE employs a trainable multi-level 3D grid structure. The position of a sampled point is encoded by interpolating the features (\mathbb{R}^F) located at the vertices of the grid cell containing the point. These interpolated features are then fed into an MLP network, predicting both the density (σ) and the point’s color (c).

The grid is organized into L levels, each containing a hash table of size $T \times F$, where T represents the number of features and F is the dimensionality of each feature. To efficiently map the grid coordinates, a spatial hash function $h(x)$, based on the approach of [53], is utilized:

$$h(x) = \left(\bigoplus_{i=1}^d x_i \pi_i \right) \bmod T \tag{3}$$

Here, \oplus denotes the bitwise XOR operation, and π_i are distinct large prime numbers.

3.2. Continual Neural Graphics Primitive (C-NGP)

This section introduces the C-NGP framework that incorporates scene-conditioning and continual learning in the Instant-NGP network [38].

Conditioning: To condition Instant-NGP, we use pseudo integer labels $C \in \{1, 2, 3, \dots\}$ to differentiate scenes. Figure 3 illustrates the information flow. To get the Neural Hash Encoding (NHE) of coordinates, we combine the scene coordinates (x, y, z) with the pseudo label (C). Additionally, the pseudo labels undergo sinusoidal positional encoding (PE) [51], denoted as $\psi \in \mathbb{R}^{2\alpha}$, where $\alpha = 2$ represents the number of frequency components used. The neural hash encoding (NHE) and encoded pseudo labels (ψ) are concatenated and passed through a single-layer MLP to obtain density (σ) and scene features. The predicted scene feature is then used to compute the color for each input coordinate (x, y, z) . Specifically, the scene feature is concatenated with the encoded viewing direction (SHE) and encoded pseudo label (ψ), forming the input to a two-layer MLP that predicts the final color values. The viewing direction is encoded using spherical harmonics encoding (SHE) [44], further refining the rendering process.

Neural hashing helps segregate scenes within a shared representation space upon scene-conditioning (features visualized in the supplementary). As shown in Figure 2, training Instant-NGP [38] on a mixed dataset without conditioning led to intermixing of scene information. This confirms that neural hashing with only scene coordinates is insufficient for distinguishing scenes in a multi-scene setting. To achieve unique scene representations, additional conditioning is required.

Continual learning: While conditioning helps non-conflicting scene representations, continual learning accommodates new unseen scenes incrementally. Therefore, the proposed C-NGP involves training Instant-NGP (with scene conditioning) in a continual learning paradigm as follows. Each scene is encoded into conditional Instant-NGP using a pseudo label. Before encoding a new scene, we first render all previously observed scenes using the camera parameters of the new scene. These rendered images are then added to the training set of the new scene, and the model parameters are updated accordingly. This strategy eliminates reliance on previous training datasets while ensuring high-fidelity modeling of all observed scenes. Algorithm 1 outlines the proposed training strategy for C-NGP. Rendering previously seen scenes with updated camera parameters is particularly effective for datasets like NeRF Synthetic 360°. For other scene types, we use the stored camera parameters for rendering.

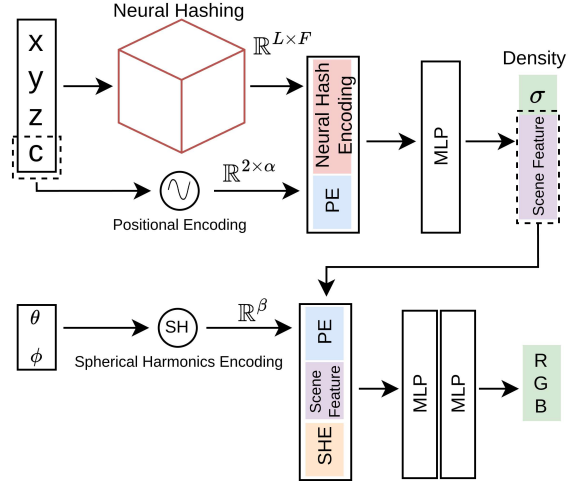


Figure 3. **Conditioning and Continual Learning for Multi-scene Modeling.** Our modification to the Instant-NGP architecture [38] enables multi-scene modeling using pseudo labels. These labels are encoded with neural hashing and scene coordinates and then processed with positional encoding. The resulting representation is concatenated with the neural hash features, enhancing performance as demonstrated in the ablation study (supp.).

3.3. Loss and Regularization

Floateres represent a significant challenge in radiance fields, typically manifesting as disconnected, dense spatial regions near the camera plane. Therefore, apart from the conventional rendering loss \mathcal{L}_{mse} , we include two additional regularizations to ensure stable C-NGP training.

Distortion. Following the work of [4, 64], we used distortion loss for compact point distribution on the camera ray:

$$\mathcal{L}_{dist} = \frac{1}{d(r)} \left(\sum_i w_i w_j \left| \frac{t_i + t_{i+1}}{2} - \frac{t_j + t_{j+1}}{2} \right| + \frac{1}{3} \sum_{i=1}^N w_i^2 (t_{i+1} - t_i) \right) \quad (4)$$

where, $d(r) = \frac{\sum_{i=1}^N w_i t_i}{\sum_{i=1}^N w_i}$ is depth along each ray. The first part of \mathcal{L}_{dist} minimizes the weighted distance between all pairs of interval midpoints. The second part focuses on minimizing the weighted size of each interval. Jointly, the weights on the ray are encouraged to be compact by pulling distance intervals closer by consolidating each weight and minimizing the width of each interval [4].

Ray entropy. The entropy regularization calculates the entropy of the ray’s distribution [5, 24] for each ray passing through the scene. This involves assessing the uncertainty or randomness in the predicted densities along the ray and avoiding the floaters in the rendered scene. The entropy

Algorithm 1: Learning new scenes using Conditional-cum-Continual NeRF (C-NGP)

Require: I_{new} : list of new scene images
Require: l_{new} : pseudo label for new scene
Require: L_{prev} : list of pseudo labels for previous scenes
Require: F_θ : NeRF network
Require: $C_{I_{new}}$: camera parameters of new scene
Require: k : number of images to render for previous scenes

```
/* Render previous scenes and store in  $I_{prev}$ 
*/
Initialize  $I_{prev} \leftarrow \{\}$ 
for  $l_{prev}^i \in L_{prev}$  do
  render_image  $\leftarrow F_\theta(l_{prev}^i, C_{I_{new}}, k)$ 
   $I_{prev}.append(render\_image)$ 
 $T_{images} \leftarrow concat(I_{new}, I_{prev})$  // train images
list
 $T_{labels} \leftarrow concat(L_{new}, L_{prev})$  // train labels
list
/* TrainNeRF() train the  $F_\theta$  on given scene
list and labels */
 $F_\theta^{updated} \leftarrow$ 
  TrainNeRF( $F_\theta, T_{images}, T_{labels}, C_{I_{new}}$ )
Output: Updated  $F_\theta^{updated}$  on new scene
```

regularization is described as per Equation 5

$$\mathcal{L}_{ent} = \left(- \sum_{i=1}^N p(r_i) \log(p(r_i)) \right) \quad (5)$$

Here, N is the number of sampled points on the ray r , and p_i is the opacity of each sampled point.

Complete loss. To train the C-NGP method, we used the combined loss formulation, as described in Equation 6.

$$\mathcal{L}_{total} = \mathcal{L}_{mse} + \lambda_{ent} \mathcal{L}_{ent} + \lambda_{dist} \mathcal{L}_{dist} \quad (6)$$

Here, λ_{ent} and λ_{dist} are the weights for the regularization. We keep these parameters for training the complete network as $\lambda_{ent} = 1e - 3$ and $\lambda_{dist} = 1e - 2$.

4. Experiments

In this section, we perform an exhaustive set of experiments to demonstrate the efficacy of the proposed framework. We start by discussing the datasets, evaluation metrics, and comparison baselines.

4.1. Datasets and Evaluation Metrics

We evaluate our model on widely used datasets: NeRF Synthetic 360° [37], Tanks and Temples [26], and Forward-

Facing LLFF [36]. NeRF Synthetic 360° consists of eight diverse scenes, each with 100 training views and 200 test views at a resolution of 800×800 . The images are rendered from either an upper hemisphere or a full hemisphere, and the camera parameters are not necessarily consistent across scenes. Forward-Facing LLFF contains eight real-world scenes captured with a handheld camera in a forward-facing manner. The number of images per scene varies from 20 to 62, with a resolution of 1008×756 . Tanks and Temples feature five large-scale scenes with complex geometries and real-world objects, each captured at a resolution of 1920×1080 . We use the masked version of this dataset for training and testing, following [32].

Additionally, we generate a dataset of 22 scenes using BlenderNeRF [43]. Each scene is created from freely available 3D object meshes and rendered with 100 training views and 100 test views from an upper hemisphere. This dataset is designed to stress test the continual learning setup of C-NGP and analyze the representative upper bound of network parameters. Further details on this analysis are provided in the supplementary material. To ensure fair evaluation in a continual learning setup, all scenes in this dataset are rendered with the same camera parameters.

Metrics. We quantitatively evaluate the model performance Peak-Signal-to-Noise-Ratio (PSNR) [1], Structural Similarity Index (SSIM) [62], and Perceptual Score (LPIPS) [70].

4.2. Training Details

For training C-NGP, we used a batch size of 10,000 rays and an initial learning rate of 2×10^3 . The model was trained for 30 epochs across synthetic and real datasets. C-NGP was conditioned on pseudo labels assigned to each scene to ensure scene-specific representations. The hash table size for Instant-NGP was set to $T = 2^{19}$, with a feature size of $F = 4$. For the NeRF Synthetic 360° dataset, we applied the generative replay method [47], where previously observed scenes were re-rendered using the camera parameters of the new scene. For real-world datasets like LLFF [36] and Tanks and Temples [26], which lack full 360° coverage, we stored the camera parameters of each scene. This allowed us to generate novel views while avoiding artifacts such as floaters or ghosting—less problematic issues in synthetic datasets with complete 360° coverage.

4.3. Choice of Comparison Baselines

Since no existing work incrementally models multiple scenes in a single radiance field, we compare our approach with the most closely related baselines that align, at least partially, with our experimental setup [8, 22, 59, 61]. Among them, SCARF [61] is the closest and most concurrent to our work, as it handles multiple scenes by increasing the number of parameters through a global parameter generator. However,

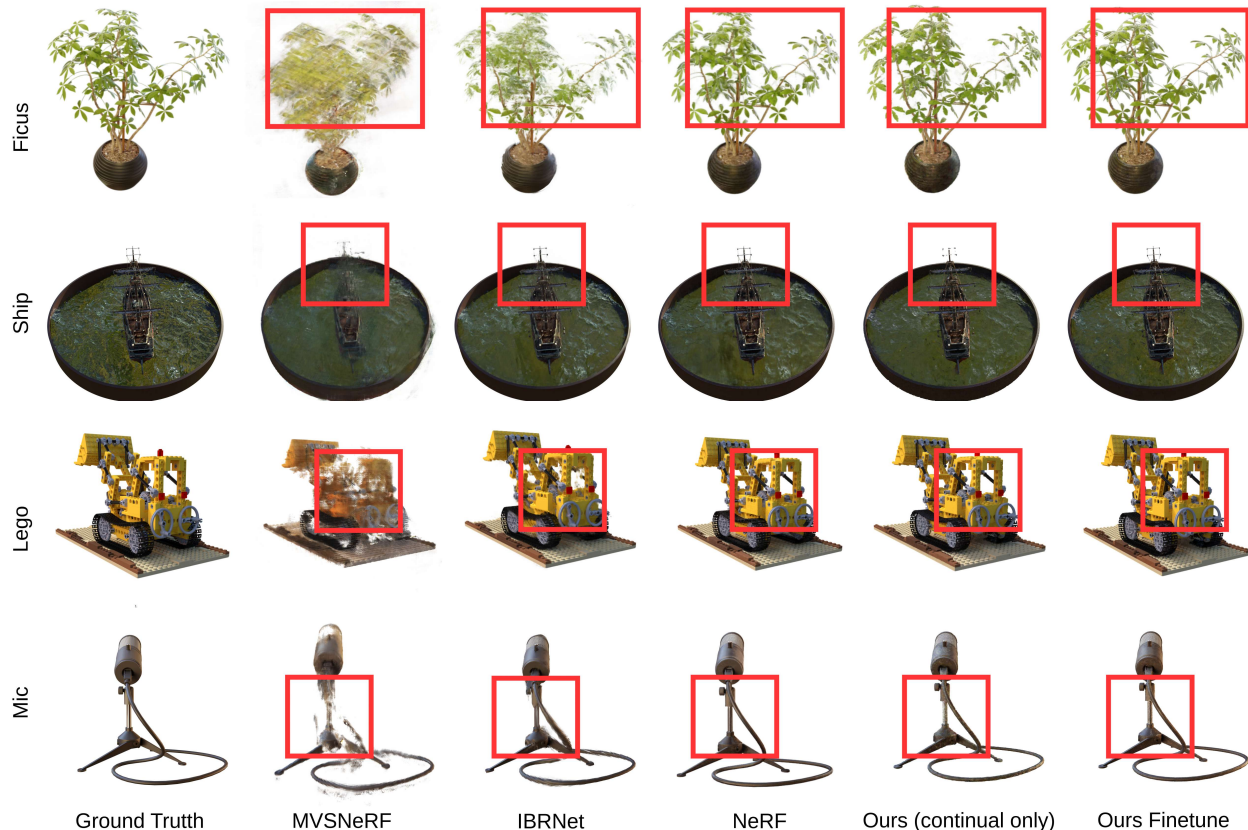


Figure 4. Qualitative Comparison on the NeRF Synthetic 360° dataset [37]. C-NGP is compared with MVSNeRF [8] and IBRNet [59] (both with per-scene fine-tuning), and vanilla NeRF [37] with per-scene optimization. C-NGP is observed to model scenes with minimal artifacts compared to those present in the other methods. The quality is enhanced further upon additional per-scene fine-tuning over C-NGP. The marked regions highlight the differences and are best viewed in PDF with Zoom.

we could not compare the performance with SCARF due to the unavailability of their code. MVSNeRF [8], IBRNet [59], and CP-NeRF [22] focus on generalizing NeRF to unseen scenes using different conditioning mechanisms. These include CNN-based feature extraction [59], 3D cost volume features [8], and meta-learning a hyper-network to generate NeRF MLP weights [22]. Since scene generalization can be interpreted as the ability to model multiple unseen scenes through feature-based conditioning, we use these methods as our baselines. For a fair comparison, we also adapt our continual learning paradigm to vanilla NeRF [37], referred to as NeRF*. We compare MVSNeRF [8], IBRNet [59], and NeRF* both qualitatively and quantitatively. We could only perform a quantitative comparison with CP-NeRF [22] due to the unavailability of their trained weights.

4.4. Experimental Setup

The baseline methods report performance under two experimental settings: *with* and *without finetuning*. (a)

Without finetuning: The model is trained on a set of scenes and evaluated on test scenes without modifying the learned parameters. (b) *With finetuning*: The model is first trained

on a set of scenes, then fine-tuned on training images of a specific scene for a few epochs before evaluation on its unseen views. Although finetuning may seem redundant, as the model has already seen those scenes and will naturally perform better, we introduce it for a fair comparison similar to CP-NeRF [22], which also reports performance after finetuning on specific scenes.

To ensure a fair comparison with C-NGP, we determine the best setting for each baseline. Since MVSNeRF [8] and IBRNet [59] are not trained on scenes from NeRF Synthetic [37] or Real forward-facing [36], we compare MVSNeRF and IBRNet *with finetuning* over these datasets. In contrast, NeRF*, CP-NeRF [22], and C-NGP are optimized on scenes from these datasets and are evaluated *without fine-tuning*.

Notably, if the training data of previously observed scenes is available, fine-tuning C-NGP on those scenes can further improve rendering quality. However, as we will see, even without finetuning, C-NGP delivers significantly better results than the baselines. The results are summarized in Table 1 and Table 2 for the NeRF Synthetic 360° [37] and Real forward-facing [36] datasets, respectively.

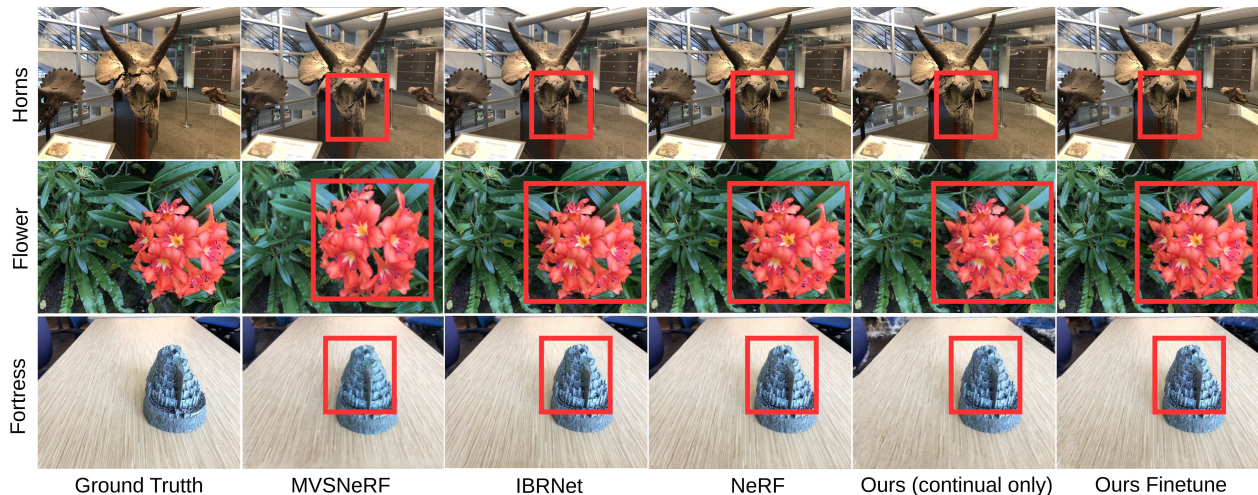


Figure 5. Qualitative Comparison on the Real Forward Facing (LLFF) dataset [36]. We compare C-NGP with MVSNeRF [8] and IBRNet [59] (both with per-scene fine-tuning), and vanilla NeRF [37] with per-scene. C-NGP performs nearly equivalent to vanilla NeRF and performs better upon per-scene fine-tuning. The marked regions show the differences and are best viewed in PDF with Zoom.

Method	Finetuning	NeRF Synthetic 360°		
		PSNR \uparrow	SSIM \uparrow	LPIPS \downarrow
NeRF*	x	21.75	0.84	0.16
IBRNet [59]	\checkmark	28.14	0.94	0.07
MVSNeRF [8]	\checkmark	27.07	0.93	0.17
CP-NeRF [22]	x	29.54	0.92	0.09
C-NGP (ours)	x	29.40	0.94	0.09
CP-NeRF [22]	\checkmark	31.77	0.95	0.06
C-NGP (ours)	\checkmark	32.08	0.95	0.06

Table 1. Quantitative comparison on NeRF Synthetic 360° dataset [37] across different baseline methods. Our continual framework shows competitive performance with multi-scene modeling and even outperforms the previous state-of-the-art methods. NeRF* indicates vanilla NeRF trained under the proposed continual setup.

4.5. Quantitative Analysis

C-NGP achieves the best SSIM and LPIPS scores, with a slightly reduced PSNR (by 0.14 units compared to CP-NeRF) *without finetuning* even while modeling all the scenes of NeRF Synthetic 360°, as shown in Table 1. However, over scenes from LLFF dataset [36], C-NGP does not achieve the best scores. This is primarily due to the inherent struggle of Instant-NGP backbone on forward-facing scenes, as observed when compared even to vanilla NeRF [37] (see Table 2, Row 4 & 5). However, after finetuning, it surpasses Instant-NGP (Table 2, Row 8). Please note that Instant-NGP was chosen as a backbone for its fast training benefits. We also evaluate vanilla NeRF in a continual setting to assess the multi-scene capabilities of radiance fields in general (Table 1, Row 1). Unlike baselines, C-NGP incrementally learns multiple scenes without expanding the model size. SCARF [61] achieves continual learning by growing parameters per scene, while C-NGP maintains a fixed parameter count. We also

Method	Finetuning	Real Forward-Facing		
		PSNR \uparrow	SSIM \uparrow	LPIPS \downarrow
IBRNet [59]	\checkmark	26.73	0.85	0.18
MVSNeRF [8]	\checkmark	25.45	0.88	0.19
CP-NeRF [22]	x	25.41	0.77	0.20
NeRF [37]	per-scene opt.	26.50	0.81	0.25
Instant-NGP [38]	per scene opt.	24.98	0.78	0.24
C-NGP (ours)	x	22.12	0.66	0.37
CP-NeRF [22]	\checkmark	27.23	0.81	0.14
C-NGP (ours)	\checkmark	25.19	0.76	0.25

Table 2. Quantitative comparison on Real Forward Facing dataset [36] across different baseline methods. We compare C-NGP with Instant-NGP (highlighted in red) and vanilla NeRF. The performance of C-NGP is constrained by that of the Instant-NGP backbone, whose performance falls short of vanilla NeRF itself on the LLFF dataset. However, additional fine-tuning boosts C-NGP’s performance.

compare the proposed paradigm against the continual learning frameworks using Elastic Weight Consolidation (EWC), PacketNet [33], and single-scene continual NeRF methods like MEIL-NeRF [13] and CLNeRF [47]. On Tanks and Temples [26], C-NGP achieves the highest PSNR and SSIM comparable to SCARF (0.02 units lower) while avoiding additional parameters per scene (Table 3).

4.6. Qualitative Analysis

We qualitatively evaluate the visual fidelity of multiple scenes rendered by C-NGP across the NeRF Synthetic [36] and Real Forward-Facing [36] datasets in Figures 9 and 10, respectively. The visuals from Tanks and Temples [26] are provided in supplementary. Additionally, we provide a qualitative comparison with MVSNeRF [8], IBRNet [59], and vanilla NeRF [37] in Figures 4 and 5. Given its multi-scene modeling capability, we expect C-NGP’s performance to at

Method	Tanks and Temples	
	PSNR \uparrow	SSIM \uparrow
EWC [25] + NeRF	15.64	0.420
PackNet [33] + NeRF	16.71	0.547
MEIL-NeRF [13]	17.98	0.580
CLNeRF [47]	21.30	0.640
SCARF [61]	26.78	0.89
C-NGP (ours)	26.93	0.87

Table 3. Quantitative comparison of C-NGP on the Tanks and Temple dataset [26] with baselines that combine either conventional continual learning methods with NeRF or introduce continual learning for single scene optimization along with a concurrent work.

least closely match per-scene optimized vanilla NeRF. Our results show that C-NGP achieves the best rendering quality on the NeRF Synthetic dataset and closely matches vanilla NeRF (which performs better than Instant-NGP) on the Real Forward-Facing dataset [36].

4.7. Stylizing 3D Scenes

To show the application of the proposed C-NGP framework, we adapt it for style editing in 3D scenes [23, 27, 39]. The current methods are only able to do single style transfer to any NeRF model at a time [18, 21], and for each new style, they have to train the NeRF model again. The incremental nature of C-NGP also allows for accommodating multiple different styles within a scene. For each scene, we train a separate C-NGP network $\theta^1, \theta^2, \theta^3, \theta^4$ and for each θ^i , we first learn the same scene for K times incrementally using C-NGP and to transfer the style, we only fine-tune the MLP layer responsible for color (RGB). As shown in Figure 6, we learn two different styles for each scene, i.e., each θ^i stores three different variations of the same scene, where the first is the original scene itself, and the next two are the edited scene styles which are vintage and anime. To generate consistent multi-view style scenes for training, we follow the work by Fujiwara *et al.* [18], which uses fully fused attention and depth-conditioned ControlNet [69].

4.8. Time Analysis

Training time and rendering speed are crucial factors when modeling multiple scenes. As shown in Table 4, NeRF requires 12 days to train and 30 seconds per frame to render, making it impractical. Other methods like MVSNeRF [8] and IBRNet [59] reduce training time but still have long fine-tuning and rendering times. In contrast, C-NGP trains in just 8 hours, fine-tuning takes 10 minutes per scene, and renders at 1.2 seconds per frame, making it highly efficient for real-time applications.

Supplementary. Due to space constraints, we discuss the following aspects of our study in the supplementary material. (a) Progressive degradation of rendering quality with each newly added scene, (b) offline vs. online sampling based on the availability of the training data of previously learned

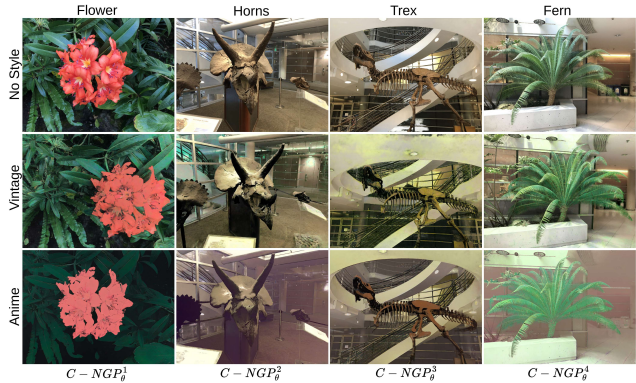


Figure 6. **Style 3D Scene.** The figure illustrates how the proposed C-NGP method stores multiple edit styles within a single network. Each scene is trained separately, represented by θ^i , and stores different edit styles for respective scenes.

Method	Training Time/ Complete Dataset	Fine-tuning Time/ Scene	Rendering Time/ Frame
NeRF*	~ 12 days	x	~ 30 sec
MVSNeRF [8]	x	~ 1 hour	~ 14 sec
IBRNet [59]	x	~ 9 hours	~ 18 sec
CP-NeRF [22]	> 2 days	x	x
C-NGP (ours)	~ 8 hours	~ 10 mins	~ 1.2 sec

Table 4. **Time Comparison.** Training, fine-tuning and rendering time comparison of C-NGP with other methods on the dataset NeRF Synthetic 360° . All time comparison experiments are done on NVIDIA RTX Quadro 5000 GPU. NeRF* indicates vanilla NeRF trained under the proposed continual learning setup.

scenes, (c) effect of camera parameters, (d) ablation studies, (e) upper bound of C-NGP *i.e.* the maximum number of scenes it can model with an acceptable loss in rendering quality and (f) shared feature space visualization and more qualitative results.

5. Conclusion

We introduced C-NGP, a continual learning framework for incremental multi-scene modeling within a single neural radiance field. C-NGP accommodates new scenes while reasonably preserving the previously learned information via scene conditioning and generative replay. Extensive empirical studies on synthetic and real datasets demonstrate that C-NGP achieves strong performance in multi-scene representation learning and outperforms existing methods over training and inference speed, offering real-time rendering capabilities. While at this stage, C-NGP incurs an acceptable loss in rendering quality while modeling multiple scenes, its performance in highly diverse scene settings and attempt towards zero forgetting warrants further exploration.

References

- [1] Implementation of a modified cvsd coder. *International Journal of Electronics*, 62(3):473–479, 1987. 5

- [2] Chong Bao, Yinda Zhang, Bangbang Yang, Tianxing Fan, Zesong Yang, Hujun Bao, Guofeng Zhang, and Zhaopeng Cui. Sine: Semantic-driven image-based nerf editing with prior-guided editing field. In *Proceedings of the IEEE/CVF Conference on Computer Vision and Pattern Recognition*, pages 20919–20929, 2023. 1, 2
- [3] Yanqi Bao, Tianyu Ding, Jing Huo, Wenbin Li, Yuxin Li, and Yang Gao. Insertnerf: Instilling generalizability into nerf with hypernet modules. *arXiv preprint arXiv:2308.13897*, 2023. 2
- [4] Jonathan T Barron, Ben Mildenhall, Dor Verbin, Pratul P Srinivasan, and Peter Hedman. Mip-nerf 360: Unbounded anti-aliased neural radiance fields. In *Proceedings of the IEEE/CVF Conference on Computer Vision and Pattern Recognition*, pages 5470–5479, 2022. 2, 4
- [5] Matteo Bonotto, Luigi Sarrocco, Daniele Evangelista, Marco Imperoli, and Alberto Pretto. Combinerf: A combination of regularization techniques for few-shot neural radiance field view synthesis. *arXiv preprint arXiv:2403.14412*, 2024. 4
- [6] Andrew Brock, Theodore Lim, James M Ritchie, and Nick Weston. Generative and discriminative voxel modeling with convolutional neural networks. *arXiv preprint arXiv:1608.04236*, 2016. 2
- [7] Zhipeng Cai and Matthias Müller. Clnrf: Continual learning meets nerf. In *Proceedings of the IEEE/CVF International Conference on Computer Vision*, pages 23185–23194, 2023. 2, 3
- [8] Anpei Chen, Zexiang Xu, Fuqiang Zhao, Xiaoshuai Zhang, Fanbo Xiang, Jingyi Yu, and Hao Su. Mvsnerf: Fast generalizable radiance field reconstruction from multi-view stereo. In *Proceedings of the IEEE/CVF international conference on computer vision*, pages 14124–14133, 2021. 2, 5, 6, 7, 8, 3
- [9] Anpei Chen, Zexiang Xu, Andreas Geiger, Jingyi Yu, and Hao Su. Tensorf: Tensorial radiance fields. In *European conference on computer vision*, pages 333–350. Springer, 2022. 1
- [10] Jianchuan Chen, Wentao Yi, Liqian Ma, Xu Jia, and Huchuan Lu. Gm-nerf: Learning generalizable model-based neural radiance fields from multi-view images. In *Proceedings of the IEEE/CVF Conference on Computer Vision and Pattern Recognition*, pages 20648–20658, 2023. 1, 2
- [11] Yue Chen, Xingyu Chen, Xuan Wang, Qi Zhang, Yu Guo, Ying Shan, and Fei Wang. Local-to-global registration for bundle-adjusting neural radiance fields. In *Proceedings of the IEEE/CVF Conference on Computer Vision and Pattern Recognition*, pages 8264–8273, 2023. 3
- [12] Zhiqin Chen, Thomas Funkhouser, Peter Hedman, and Andrea Tagliasacchi. Mobilenerf: Exploiting the polygon rasterization pipeline for efficient neural field rendering on mobile architectures. In *Proceedings of the IEEE/CVF Conference on Computer Vision and Pattern Recognition*, pages 16569–16578, 2023. 1, 2
- [13] Jaeyoung Chung, Kanggeon Lee, Sungyong Baik, and Kyoung Mu Lee. Meil-nerf: Memory-efficient incremental learning of neural radiance fields. *arXiv preprint arXiv:2212.08328*, 2022. 2, 3, 7, 8
- [14] Paul E Debevec, Camillo J Taylor, and Jitendra Malik. Modeling and rendering architecture from photographs: A hybrid geometry-and image-based approach. In *Seminal Graphics Papers: Pushing the Boundaries, Volume 2*, pages 465–474, 2023. 2
- [15] Tianchen Deng, Guole Shen, Tong Qin, Jianyu Wang, Wentao Zhao, Jingchuan Wang, Danwei Wang, and Weidong Chen. Pglslam: Progressive neural scene representation with local to global bundle adjustment. In *Proceedings of the IEEE/CVF Conference on Computer Vision and Pattern Recognition*, pages 19657–19666, 2024. 3
- [16] Shuangfang Fang, Weixin Xu, Heng Wang, Yi Yang, Yufeng Wang, and Shuchang Zhou. One is all: Bridging the gap between neural radiance fields architectures with progressive volume distillation. In *Proceedings of the AAAI Conference on Artificial Intelligence*, pages 597–605, 2023. 1
- [17] Sara Fridovich-Keil, Alex Yu, Matthew Tancik, Qinhong Chen, Benjamin Recht, and Angjoo Kanazawa. Plenoxels: Radiance fields without neural networks. In *Proceedings of the IEEE/CVF Conference on Computer Vision and Pattern Recognition*, pages 5501–5510, 2022. 1, 2
- [18] Haruo Fujiwara, Yusuke Mukuta, and Tatsuya Harada. Style-nerf2nerf: 3d style transfer from style-aligned multi-view images. In *SIGGRAPH Asia 2024 Conference Papers*, pages 1–10, 2024. 8
- [19] Cameron Gordon, Shin-Fang Chng, Lachlan MacDonald, and Simon Lucey. On quantizing implicit neural representations. In *Proceedings of the IEEE/CVF Winter Conference on Applications of Computer Vision*, pages 341–350, 2023. 1
- [20] Steven J Gortler, Radek Grzeszczuk, Richard Szeliski, and Michael F Cohen. The lumigraph. In *Seminal Graphics Papers: Pushing the Boundaries, Volume 2*, pages 453–464, 2023. 2
- [21] Ayaan Haque, Matthew Tancik, Alexei A Efros, Aleksander Holynski, and Angjoo Kanazawa. Instruct-nerf2nerf: Editing 3d scenes with instructions. In *Proceedings of the IEEE/CVF International Conference on Computer Vision*, pages 19740–19750, 2023. 8
- [22] Hao He, Yixun Liang, Shishi Xiao, Jierun Chen, and Yingcong Chen. Cp-nerf: Conditionally parameterized neural radiance fields for cross-scene novel view synthesis. In *Computer Graphics Forum*, page e14940. Wiley Online Library, 2023. 1, 2, 5, 6, 7, 8
- [23] Hsin-Ping Huang, Hung-Yu Tseng, Saurabh Saini, Maneesh Singh, and Ming-Hsuan Yang. Learning to stylize novel views. In *Proceedings of the IEEE/CVF International Conference on Computer Vision*, pages 13869–13878, 2021. 8
- [24] Mijeong Kim, Seonguk Seo, and Bohyung Han. Infonerf: Ray entropy minimization for few-shot neural volume rendering. In *Proceedings of the IEEE/CVF Conference on Computer Vision and Pattern Recognition*, pages 12912–12921, 2022. 4
- [25] James Kirkpatrick, Razvan Pascanu, Neil Rabinowitz, Joel Veness, Guillaume Desjardins, Andrei A Rusu, Kieran Milan, John Quan, Tiago Ramalho, Agnieszka Grabska-Barwinska, et al. Overcoming catastrophic forgetting in neural networks. *Proceedings of the national academy of sciences*, 114(13): 3521–3526, 2017. 3, 8
- [26] Arno Knapitsch, Jaesik Park, Qian-Yi Zhou, and Vladlen Koltun. Tanks and temples: Benchmarking large-scale scene

- reconstruction. *ACM Transactions on Graphics (ToG)*, 36(4): 1–13, 2017. 5, 7, 8
- [27] Georgios Kopanas, Julien Philip, Thomas Leimkühler, and George Drettakis. Point-based neural rendering with per-view optimization. In *Computer Graphics Forum*, pages 29–43. Wiley Online Library, 2021. 8
- [28] SeokYeong Lee, JunYong Choi, Seungryong Kim, Ig-Jae Kim, and Junghyun Cho. Few-shot neural radiance fields under unconstrained illumination. In *Proceedings of the AAAI Conference on Artificial Intelligence*, pages 2938–2946, 2024. 1, 2
- [29] Marc Levoy and Pat Hanrahan. Light field rendering. In *Seminal Graphics Papers: Pushing the Boundaries, Volume 2*, pages 441–452. 2023. 2
- [30] Zhizhong Li and Derek Hoiem. Learning without forgetting. *IEEE transactions on pattern analysis and machine intelligence*, 40(12):2935–2947, 2017. 3
- [31] Yiyi Liao, Simon Donne, and Andreas Geiger. Deep marching cubes: Learning explicit surface representations. In *Proceedings of the IEEE Conference on Computer Vision and Pattern Recognition*, pages 2916–2925, 2018. 2
- [32] Lingjie Liu, Jiatao Gu, Kyaw Zaw Lin, Tat-Seng Chua, and Christian Theobalt. Neural sparse voxel fields. *Advances in Neural Information Processing Systems*, 33:15651–15663, 2020. 5
- [33] Arun Mallya and Svetlana Lazebnik. Packnet: Adding multiple tasks to a single network by iterative pruning. In *Proceedings of the IEEE conference on Computer Vision and Pattern Recognition*, pages 7765–7773, 2018. 3, 7, 8
- [34] Nelson Max. Optical models for direct volume rendering. *IEEE Transactions on Visualization and Computer Graphics*, 1(2):99–108, 1995. 3
- [35] Lars Mescheder, Michael Oechsle, Michael Niemeyer, Sebastian Nowozin, and Andreas Geiger. Occupancy networks: Learning 3d reconstruction in function space. In *Proceedings of the IEEE/CVF conference on computer vision and pattern recognition*, pages 4460–4470, 2019. 2
- [36] Ben Mildenhall, Pratul P Srinivasan, Rodrigo Ortiz-Cayon, Nima Khademi Kalantari, Ravi Ramamoorthi, Ren Ng, and Abhishek Kar. Local light field fusion: Practical view synthesis with prescriptive sampling guidelines. *ACM Transactions on Graphics (ToG)*, 38(4):1–14, 2019. 2, 5, 6, 7, 8, 4
- [37] Ben Mildenhall, Pratul P Srinivasan, Matthew Tancik, Jonathan T Barron, Ravi Ramamoorthi, and Ren Ng. Nerf: Representing scenes as neural radiance fields for view synthesis. *Communications of the ACM*, 65(1):99–106, 2021. 1, 2, 3, 5, 6, 7, 4
- [38] Thomas Müller, Alex Evans, Christoph Schied, and Alexander Keller. Instant neural graphics primitives with a multiresolution hash encoding. *ACM transactions on graphics (TOG)*, 41(4):1–15, 2022. 2, 3, 4, 7
- [39] Thu Nguyen-Phuoc, Feng Liu, and Lei Xiao. Snerf: stylized neural implicit representations for 3d scenes. *arXiv preprint arXiv:2207.02363*, 2022. 8
- [40] Michael Niemeyer, Lars Mescheder, Michael Oechsle, and Andreas Geiger. Differentiable volumetric rendering: Learning implicit 3d representations without 3d supervision. In *Proceedings of the IEEE/CVF conference on computer vision and pattern recognition*, pages 3504–3515, 2020. 2
- [41] Jeong Joon Park, Peter Florence, Julian Straub, Richard Newcombe, and Steven Lovegrove. Deepsdf: Learning continuous signed distance functions for shape representation. In *Proceedings of the IEEE/CVF conference on computer vision and pattern recognition*, pages 165–174, 2019. 2
- [42] Ryan Po, Zhengyang Dong, Alexander W Bergman, and Gordon Wetzstein. Instant continual learning of neural radiance fields. In *Proceedings of the IEEE/CVF International Conference on Computer Vision*, pages 3334–3344, 2023. 2, 3
- [43] Maxime Raafat. GitHub - maximeraafat/BlenderNeRF: Easy NeRF synthetic dataset creation within Blender — github.com. <https://github.com/maximeraafat/BlenderNeRF>. [Accessed 19-05-2024]. 5
- [44] Ravi Ramamoorthi and Pat Hanrahan. An efficient representation for irradiance environment maps. In *Proceedings of the 28th annual conference on Computer graphics and interactive techniques*, pages 497–500, 2001. 4
- [45] Amal Rannen, Rahaf Aljundi, Matthew B Blaschko, and Tinne Tuytelaars. Encoder based lifelong learning. In *Proceedings of the IEEE international conference on computer vision*, pages 1320–1328, 2017. 3
- [46] Anthony Robins. Catastrophic forgetting, rehearsal and pseudorehearsal. *Connection Science*, 7(2):123–146, 1995. 3
- [47] Hanul Shin, Jung Kwon Lee, Jaehong Kim, and Jiwon Kim. Continual learning with deep generative replay. *Advances in neural information processing systems*, 30, 2017. 3, 5, 7, 8
- [48] Seungjoo Shin and Jaesik Park. Binary radiance fields. *Advances in neural information processing systems*, 36, 2024. 1
- [49] David Stutz and Andreas Geiger. Learning 3d shape completion from laser scan data with weak supervision. In *Proceedings of the IEEE conference on computer vision and pattern recognition*, pages 1955–1964, 2018. 2
- [50] Edgar Sucar, Shikun Liu, Joseph Ortiz, and Andrew J Davison. imap: Implicit mapping and positioning in real-time. In *Proceedings of the IEEE/CVF international conference on computer vision*, pages 6229–6238, 2021. 3
- [51] Matthew Tancik, Pratul Srinivasan, Ben Mildenhall, Sara Fridovich-Keil, Nithin Raghavan, Utkarsh Singhal, Ravi Ramamoorthi, Jonathan Barron, and Ren Ng. Fourier features let networks learn high frequency functions in low dimensional domains. *Advances in neural information processing systems*, 33:7537–7547, 2020. 4
- [52] Jiaxiang Tang, Xiaokang Chen, Jingbo Wang, and Gang Zeng. Compressible-composable nerf via rank-residual decomposition. *Advances in Neural Information Processing Systems*, 35:14798–14809, 2022. 1
- [53] Matthias Teschner, Bruno Heidelberger, Matthias Müller, Danat Pomerantes, and Markus H Gross. Optimized spatial hashing for collision detection of deformable objects. In *Vmv*, pages 47–54, 2003. 3
- [54] Ayush Tewari, Justus Thies, Ben Mildenhall, Pratul Srinivasan, Edgar Tretschk, Wang Yifan, Christoph Lassner, Vincent Sitzmann, Ricardo Martin-Brualla, Stephen Lombardi, et al. Advances in neural rendering. In *Computer Graphics Forum*, pages 703–735. Wiley Online Library, 2022. 2

- [55] Laurens Van der Maaten and Geoffrey Hinton. Visualizing data using t-sne. *JMLR*, 9(11), 2008. 2
- [56] Ziyu Wan, Christian Richardt, Aljaž Božič, Chao Li, Vijay Rengarajan, Seonghyeon Nam, Xiaoyu Xiang, Tuotuo Li, Bo Zhu, Rakesh Ranjan, et al. Learning neural duplex radiance fields for real-time view synthesis. In *Proceedings of the IEEE/CVF Conference on Computer Vision and Pattern Recognition*, pages 8307–8316, 2023. 1, 2
- [57] Guangcong Wang, Zhaoxi Chen, Chen Change Loy, and Ziwei Liu. Sparsenerf: Distilling depth ranking for few-shot novel view synthesis. In *Proceedings of the IEEE/CVF International Conference on Computer Vision*, pages 9065–9076, 2023. 1, 2
- [58] Peng Wang, Lingjie Liu, Yuan Liu, Christian Theobalt, Taku Komura, and Wenping Wang. Neus: Learning neural implicit surfaces by volume rendering for multi-view reconstruction. *arXiv preprint arXiv:2106.10689*, 2021. 1
- [59] Qianqian Wang, Zhicheng Wang, Kyle Genova, Pratul P Srinivasan, Howard Zhou, Jonathan T Barron, Ricardo Martin-Brualla, Noah Snavely, and Thomas Funkhouser. Ibrnet: Learning multi-view image-based rendering. In *Proceedings of the IEEE/CVF Conference on Computer Vision and Pattern Recognition*, pages 4690–4699, 2021. 1, 2, 5, 6, 7, 8, 3
- [60] Yuze Wang, Junyi Wang, Yansong Qu, and Yue Qi. Rip-nerf: learning rotation-invariant point-based neural radiance field for fine-grained editing and compositing. In *Proceedings of the 2023 ACM International Conference on Multimedia Retrieval*, pages 125–134, 2023. 1, 2
- [61] Yuze Wang, Junyi Wang, Chen Wang, Wantong Duan, Yongtang Bao, and Yue Qi. Scarf: Scalable continual learning framework for memory-efficient multiple neural radiance fields. *arXiv preprint arXiv:2409.04482*, 2024. 3, 5, 7, 8
- [62] Zhou Wang, Alan C Bovik, Hamid R Sheikh, and Eero P Simoncelli. Image quality assessment: from error visibility to structural similarity. *IEEE transactions on image processing*, 13(4):600–612, 2004. 5
- [63] Jiajun Wu, Yifan Wang, Tianfan Xue, Xingyuan Sun, Bill Freeman, and Josh Tenenbaum. Marrnet: 3d shape reconstruction via 2.5 d sketches. *Advances in neural information processing systems*, 30, 2017. 2
- [64] Jamie Wynn and Daniyar Turmukhambetov. Diffusionerf: Regularizing neural radiance fields with denoising diffusion models. In *Proceedings of the IEEE/CVF Conference on Computer Vision and Pattern Recognition*, pages 4180–4189, 2023. 4
- [65] Hao Yang, Lanqing Hong, Aoxue Li, Tianyang Hu, Zhenguo Li, Gim Hee Lee, and Liwei Wang. Contranerf: Generalizable neural radiance fields for synthetic-to-real novel view synthesis via contrastive learning. In *Proceedings of the IEEE/CVF Conference on Computer Vision and Pattern Recognition*, pages 16508–16517, 2023. 1, 2
- [66] Jiawei Yang, Marco Pavone, and Yue Wang. Freenerf: Improving few-shot neural rendering with free frequency regularization. In *Proceedings of the IEEE/CVF conference on computer vision and pattern recognition*, pages 8254–8263, 2023. 1, 2
- [67] Alex Yu, Vickie Ye, Matthew Tancik, and Angjoo Kanazawa. pixelnerf: Neural radiance fields from one or few images. In *Proceedings of the IEEE/CVF Conference on Computer Vision and Pattern Recognition*, pages 4578–4587, 2021. 1, 2
- [68] Letian Zhang, Ming Li, Chen Chen, and Jie Xu. Il-nerf: Incremental learning for neural radiance fields with camera pose alignment. *arXiv preprint arXiv:2312.05748*, 2023. 2, 3
- [69] Lvmin Zhang, Anyi Rao, and Maneesh Agrawala. Adding conditional control to text-to-image diffusion models. In *Proceedings of the IEEE/CVF international conference on computer vision*, pages 3836–3847, 2023. 8
- [70] Richard Zhang, Phillip Isola, Alexei A Efros, Eli Shechtman, and Oliver Wang. The unreasonable effectiveness of deep features as a perceptual metric. In *Proceedings of the IEEE conference on computer vision and pattern recognition*, pages 586–595, 2018. 5
- [71] Xiaoshuai Zhang, Sai Bi, Kalyan Sunkavalli, Hao Su, and Zexiang Xu. Nerfusion: Fusing radiance fields for large-scale scene reconstruction. In *Proceedings of the IEEE/CVF Conference on Computer Vision and Pattern Recognition*, pages 5449–5458, 2022. 1, 2

Incremental Multi-Scene Modeling via Continual Neural Graphics Primitives

Supplementary Material

A. Online vs. Offline Sampling and Effect of Camera Parameters

While the method does not need to have the training data of the learned scenes by design, it is worthwhile to know how well C-NGP performs with and without the availability of the actual training data, i.e., offline vs online sampling. Table 5 compares the performance of continually learning a new scene(s) using (a) the training data of the previously encountered scenes - *offline sampling* or using (b) images rendered/sampled from the trained model via the associated scene conditioning - *online sampling*. We find that the performance with *online* and *offline sampling* is nearly the same over the BlenderNeRF dataset, as shown in Table 5, Row 2. Moreover, in Table 5, Row 1, we observe that performance with *online sampling* is, in fact, better than with *offline sampling* over the NeRF Synthetic dataset [37]. We attribute such performance trends to the nature of camera parameters.

Training a neural radiance field under a continual paradigm can be best evaluated when the camera parameters across all scenes are the same because the renderings and associated ground truth images correspond to the same set of camera parameters at every stage of continual training. Interestingly, since the camera parameters of each scene in the BlenderNeRF dataset are the same, it serves as a perfect benchmark for comparing the performance under the two sampling strategies. However, a few scenes in the NeRF Synthetic 360° dataset correspond to different camera parameters. Therefore, the renderings are observed to be misaligned with respect to the ground truth images in the *offline sampling*. Figure 7 shows such misalignments due to differences in camera parameters that eventually cause a reduction in PSNR, leading to reduced performance in the offline sampling. Furthermore, due to differences in camera parameters across scenes, we observe heavier progressive degradation in the rendering quality with *offline* than with the *online sampling*. Table 6 exclusively evaluates the rendering quality of scenes from the NeRF Synthetic dataset with *offline* and *online sampling*.

B. Upper bound in C-NGP

We attempt to explore the upper bound on the number of scenes that can be accommodated within a given set of parameters with an acceptable loss in the rendering quality of the previously learned scenes. Table 7 shows the reduction in the PSNR and SSIM over scenes from a single dataset (Table 7, Column 2) and scenes from a mixed dataset, i.e., scenes from two different datasets (Table 7, Column 3). We used 22 scenes from the BlenderNeRF dataset for the single dataset.

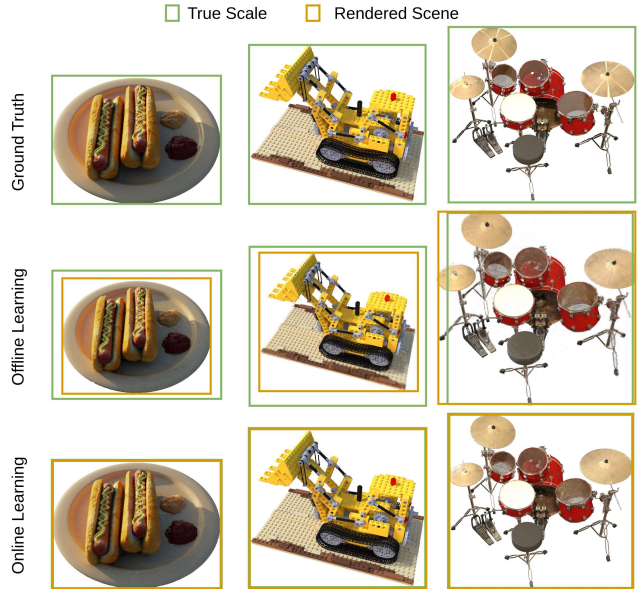


Figure 7. Effect of difference in camera parameters across scenes in the offline setting

Datasets	Offline Sampling			Online Sampling		
	PSNR \uparrow	SSIM \uparrow	LPIPS \downarrow	PSNR \uparrow	SSIM \uparrow	LPIPS \downarrow
NeRF Synthetic 360°	25.211	0.86	0.151	29.40	0.93	0.09
Blender Synthetic	37.735	0.98	0.022	37.734	0.98	0.022

Table 5. Offline vs Online sampling strategy. Analyzing the quantitative performance on training with the available training data (offline) or through images generated through the generative replay (online) while learning C-NGP. The enhanced performance with online sampling is due to the same camera parameters across all the scenes.

Moreover, for the mixed dataset, we combine 8 scenes from the NeRF-Synthetic dataset [37] and 14 scenes from the BlenderNeRF dataset to evaluate cross-dataset performance.

It is pretty evident that increasing the number of scenes for a fixed number of parameters would lead to forgetting. However, the idea here is to understand how accommodating a neural radiance field is. Therefore, we demonstrate that while we do not claim to avoid forgetting completely, most importantly, we succeed in slowing it down to the extent that we can reasonably model around ~ 20 different scenes. We observe that C-NGP can accommodate over ~ 20 different scenes with PSNR and SSIM higher than or equal to several existing NeRF variants that handle only one scene at a time

Method	Current Scene [L]				Current Scene [L → C]				Current Scene [L → C → S]				Current Scene [L → C → S → D]			
	Lego	Chair	Ship	Drums	Lego	Chair	Ship	Drums	Lego	Chair	Ship	Drums	Lego	Chair	Ship	Drums
Offline Sampling	35.62	x	x	x	34.59	34.63	x	x	34.19	34.06	28.53	x	14.41	18.12	28.06	25.02
Online Sampling	35.62	x	x	x	34.81	34.82	x	x	34.24	34.35	28.68	x	33.39	33.89	28.29	25.20

Table 6. Analysing progressive degradation in the rendering quality with *offline* and *online sampling* of scenes from the NeRF Synthetic 360° dataset [37]. The cell highlighted in red color shows high degradation in the PSNR value under offline sampling.

	Single Dataset		Mixed Dataset	
	PSNR ↑	SSIM ↑	PSNR ↑	SSIM ↑
Groups 1 (8 Scenes)	35.889	0.978	29.40	0.94
Groups 2 (12 Scenes)	33.989	0.971	28.295	0.915
Groups 3 (16 Scenes)	32.448	0.964	27.190	0.906
Groups 4 (22 Scenes)	30.472	0.954	25.744	0.896

Table 7. Analysing upper bound on the number of scenes C-NGP can accommodate with reasonable loss in rendering quality across single and mixed datasets. Single: 22 scenes from BlenderNeRF dataset. Mixed: 14 scenes from BlenderNeRF + 8 scenes from NeRF Synthetic 360° dataset.

(compare Table 7 - Row 4, Col 3 and Table 2 - Row 4, Col 3) when evaluated over the scenes from the NeRF Synthetic dataset.

Interestingly, Table 9 compares the extent of forgetting in MVSNeRF [8] and IBNet [59] with C³NeRF (not fine-tune) evaluated over the scenes in the NeRF Synthetic 360° [37] dataset. The experimental setup for the forgetting experiment is that we first fine-tune a scene on MVSNeRF and IBNet. Later, for each new scene, we use the previous scene’s fine-tuned weights and fine-tune them. For the proposed method, we follow the continual learning strategy only. No separate fine-tuning is done for C-NGP.

C. Shared Representation Space

Figure 8 shows the t-SNE map [55] of the learned multi-scene representation space of C-NGP across eight scenes from the NeRF Synthetic 360° dataset [37]. The overlapping scene clusters suggest that the parameter space is shared across multiple scenes, meaning a subset of parameters encodes shared information rather than being exclusive to a single scene.

To generate this visualization, we extract neural hash encodings (as described in Figure 3) from one image per scene, all captured from the same viewpoint. Since each image is 800 × 800 pixels and many pixels correspond to the background, we divide it into 50 × 50 patches, yielding 16 patches per image. Instead of extracting features from every pixel, we obtain MLP features from these patches across all eight scenes and visualize them using t-SNE [55].

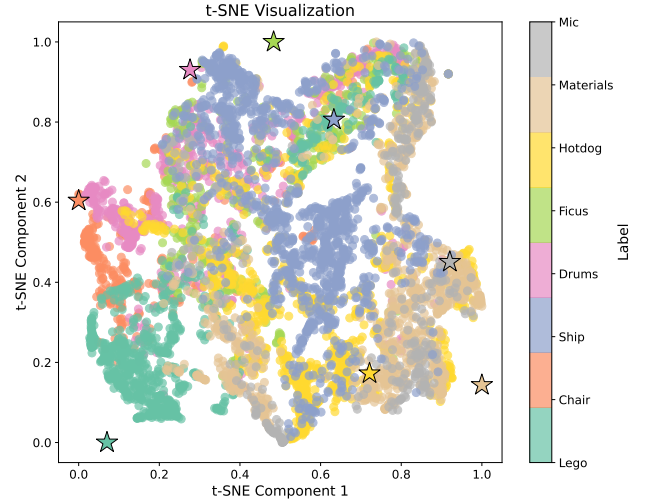


Figure 8. The figure illustrates the representation space of C-NGP, visualized through a t-SNE map over scenes from NeRF Synthetic 360° dataset [37].

Experiments	PSNR ↑	SSIM ↑	LPIPS ↓
XYZ — C + SE(θ, φ)	24.108	0.812	0.201
XYZ + ψ(C) + SE(θ, φ)	12.966	0.813	0.460
XYZ — C + ψ(C) + SE(θ, φ)	24.492	0.824	0.184
XYZ — C + ψ(C) + SE(θ, φ) + ψ(C)	25.927	0.880	0.139

Table 8. Ablation on the configuration choice for conditioning Instant-NGP network [38] - the backbone of C-NGP.

D. Ablation

We conducted an ablation study to determine the most effective way to integrate multi-scene conditioning into the Instant-NGP [38] architecture. Specifically, we evaluated different strategies for concatenating pseudo labels and their sinusoidal positional encodings with scene coordinates and viewing directions. The results are summarized in Table 8.

The baseline, XYZ — C, feeds the pseudo label alongside (x, y, z) coordinates into the neural hashing module. While straightforward, this approach relies solely on raw labels for scene differentiation. In XYZ + ψ(C), we replaced the raw label with its positional encoding ψ(C), but this led to lower performance, indicating that direct pseudo-label input is crucial for effective scene discrimination.

Adding both the raw label and its positional en-

Method	Per Scene [S, F, H, L]				Fine-tune [S → F]				Fine-tune [S → F → H]				Fine-tune [S → F → H → L]				
	Ship	Ficus	Hotdog	Lego	Ship	Ficus	Hotdog	Lego	Ship	Ficus	Hotdog	Lego	Ship	Ficus	Hotdog	Lego	Avg.
MVSNeRF [8]	21.27	19.60	22.44	18.90	12.61	17.72	x	x	15.52	16.83	18.50	x	14.63	16.75	15.80	14.43	15.40
IBRNet [59]	28.70	29.19	37.14	28.23	22.63	25.23	x	x	23.98	24.63	35.16	x	23.97	24.71	33.49	30.72	28.22
C-NGP (ours) (no fine-tuning)	30.14	33.95	37.38	35.62	28.86	32.03	x	x	28.56	31.03	35.31	x	28.06	30.61	34.62	32.31	31.4

Table 9. Comparing the extent of information forgetting in MVSNeRF [8], IBRNet [59], and C-NGP across scenes in the NeRF Synthetic 360° dataset [37].

coding ($XYZ - C + \psi(C)$) improved results, suggesting that combining these representations enhances scene modeling. The best performance was achieved with $XYZ - C + \psi(C) + SE(\theta, \phi) + \psi(C)$, where we further incorporated the spherical encoding of the viewing direction $SE(\theta, \phi)$ along with an additional instance of $\psi(C)$. This setup yielded the highest PSNR and SSIM scores and the lowest LPIPS, highlighting the benefit of jointly leveraging scene coordinates, viewing directions, and both raw and encoded labels.

Overall, our study shows that enriching multi-scene representations with positional and spherical encodings significantly improves scene modeling and retention.

E. Discussion

Empirically, we also explored the upper bound on a number of scenes that a fixed number of parameters can model. Although information forgetting can be minimized further with an increase in the number of parameters and scenes, our goal was to maximally utilize the representation capacity of a single neural radiance field parameter. Interestingly, we show that online sampling under generative replay produces better results compared to offline sampling. While the proposed framework can be viewed as taking the first steps toward multi-scene modeling, several open research avenues exist around it. An interesting future work could involve studying if the model learns useful scene priors during a continual learning process to aid in either faster learning over new scenes (*i.e.*, convergence in fewer iterations or higher initial PSNR while learning to model a new scene) or can model new scenes with fewer number of images (few-shot learning). Moreover, dissecting C-NGP or the Instant-NGP backbone to analyze the kind of scene attributes handled by the model at each layer to increase physical interpretability is also an interesting avenue to explore. With the current exploration of the representative capacity of NeRFs and the aforementioned future directions, we believe that this work could serve as a primer for a new perspective on designing multi-scene continual neural radiance fields to continue accommodating new scenes without or with minimal loss of information of previously learned scenes.

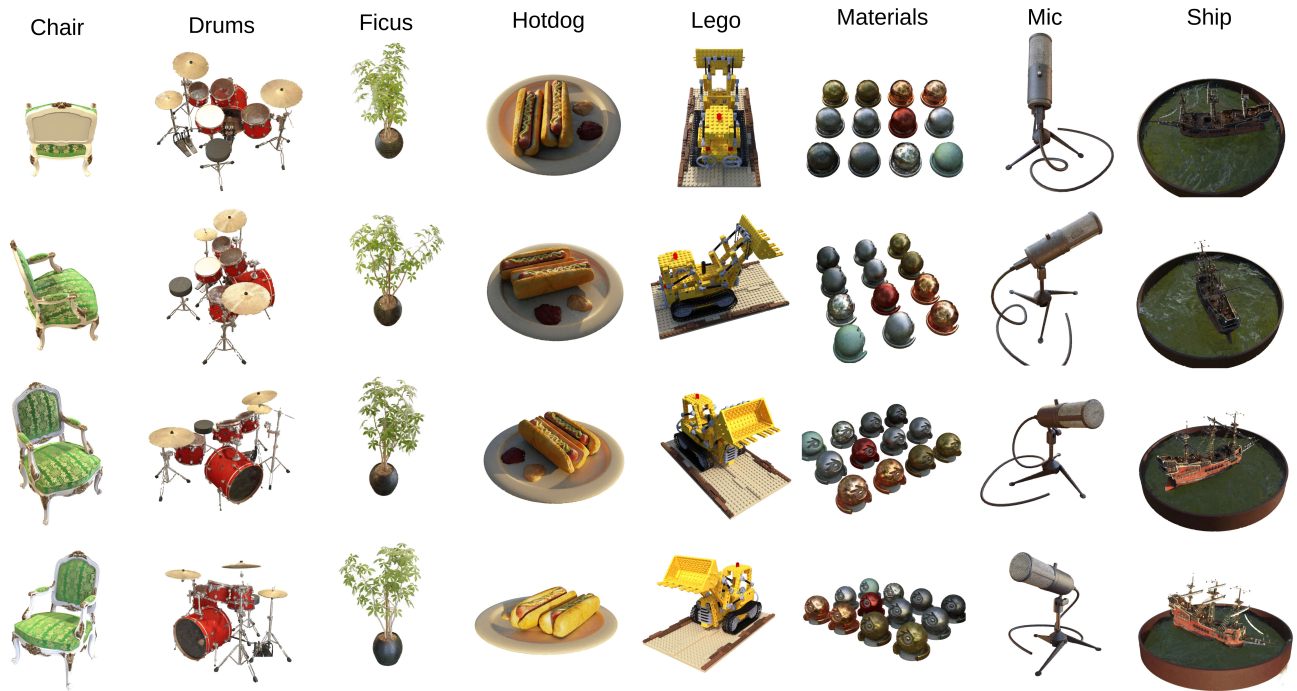


Figure 9. Qualitative demonstration of the quality of rendered images across different views through C-NGP over the scenes from the NeRF Synthetic 360° dataset [37]. It is best viewed in PDF with Zoom.

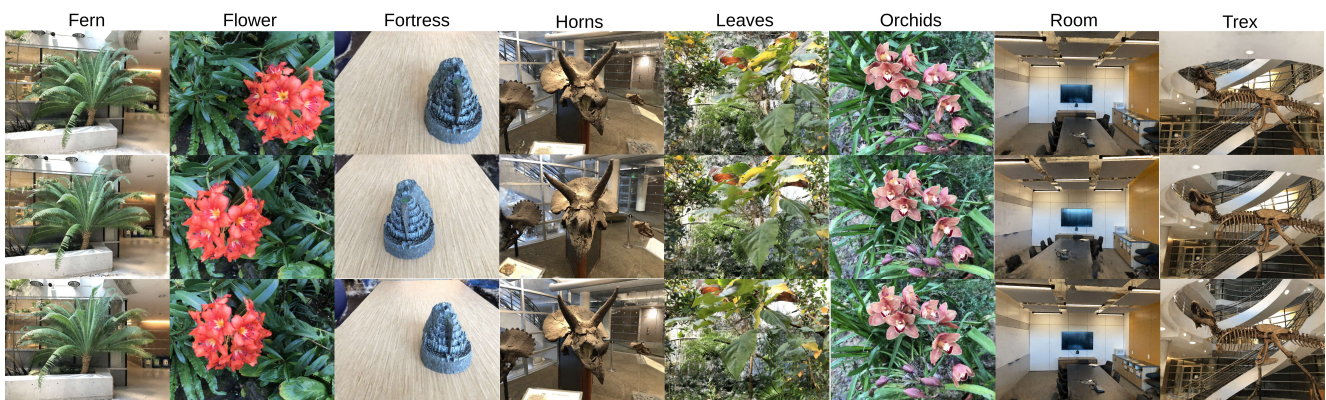


Figure 10. Qualitative demonstration of the quality of rendered images across different views through C-NGP over the scenes from the Real Forward-Facing dataset [36]. It is best viewed in PDF with Zoom.



Figure 11. Qualitative demonstration of the quality of rendered images across different views through C-NGP over the scenes from the Tanks and Temples dataset [26].